J. Fluid Mech. (2021), *vol*. 912, A1, doi:10.1017/jfm.2020.1034

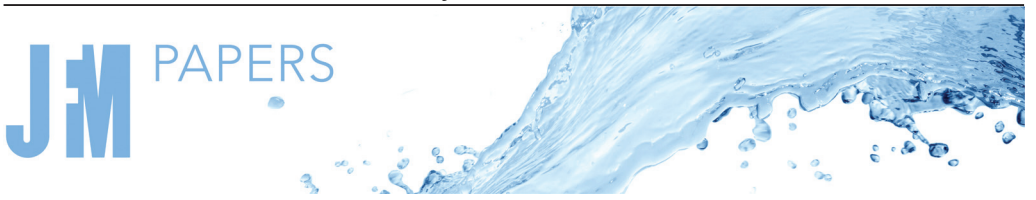

On the stratification and induced flow in an emptying–filling box driven by a plane vertically distributed source of buoyancy

Ziheng Yu[1] **and Gary R. Hunt**[1],†

[1]Department of Engineering, University of Cambridge, Trumpington Street, Cambridge CB2 1PZ, UK

(Received 9 May 2020; revised 15 September 2020; accepted 13 November 2020)

A theoretical model is presented for the steady multi-layered flow induced by a plane vertically distributed buoyancy source producing a turbulent wall plume in a ventilated box. While aspects of the stratification and rate of fluid exchange between box and exterior have been studied previously, the streamline pattern and velocity field have not been considered until now, despite having potentially important practical implications for achieving comfort in naturally ventilated buildings and for the indoor spread of airborne contagions. The boundary condition at the wall for each layer is established by deducing the turbulent entrainment rate. Using conformal mapping techniques and Poisson's integral theorem, closed-form solutions for the streamfunction of the induced flow in each layer are established. While the flow near the ceiling was overlooked in the classic model for the multi-layered stratification, after considering the possible flow scenarios, the stratification is re-evaluated herein by incorporating an entraining ceiling current. With a markedly thinner top layer, the refined stratification matches well with the available experimental observations, the restrictions we place on the applicability of the model overcoming the previous over-prediction in the number of interfaces. The magnitude of the dimensionless flow velocity, independent of the wall buoyancy flux and physical scale of the box, decreases significantly with the number of layers. Three types of layer, each with a distinct induced flow pattern, are distinguished and their implications for room airflow considered. Notably, the flow in the base layer represents a continual and smooth flushing of air between the inlet opening and the wall plume, whereas an intermediate layer is almost entirely comprised of near-stagnant air.

Key words: plumes/thermals, stratified flows

† Email address for correspondence: gary.hunt@eng.cam.ac.uk

1. Introduction

Many buoyancy sources that occur in nature and the built environment are vertically distributed. Examples include a wall exposed to sunlight, a wall separating a room on fire from one at risk, a panel heater in a room and a vertical submerged ice wall of a glacier (Heiselberg & Sandberg 1990; Linden 1999; Kerr & McConnochie 2015). The wall plume that develops adjacent to such a plane source, also referred to as a natural convection boundary layer, has been investigated extensively for an infinite wall in unbounded environments (George Jr. & Capp 1979; Tsuji & Nagano 1989; McBain, Armfield & Desrayaud 2007; Abedin, Tsuji & Hattori 2009). These studies primarily focus on the details of the flow within the wall plume. Motivated by the spread of airborne contaminants, such as a virus from a common cold or influenza, Loganathan & Hunt (2019) examine the flow induced in the ambient by a turbulent wall plume and develop an analytical solution that shows clearly delineated regions of accelerating and decelerating flow. Herein, we develop a closed-form solution for the complex pattern of stratified flow induced by a turbulent wall plume in a ventilated room, sharing the same motivation to enhance our understanding of airflow and contaminant movement in naturally ventilated rooms.

Turbulent wall plumes have also been intensively studied in confined spaces such as in a box in which the vertical plane source covers an entire internal wall of area $H \times L$, with H denoting the box height. This situation has clear practical applications, for example to the heating of a room. As a successor of the original 'emptying–filling-box' model proposed by Linden, Lane-Serff & Smeed (1990), who considered a vertical line source extending from floor to ceiling in a ventilated container, Cooper & Hunt (2010) studied both sealed and ventilated boxes with a vertical plane source. By extending the 'filling-box' theory of Baines & Turner (1969), they found that in a sealed box, both the transient and asymptotic flow features, such as the descent of the 'first front' and uniform heating at large time, were qualitatively similar to those produced by a localised source on the base. In a ventilated box, with openings at the base (of area per unit length a_l) and top (of area per unit length a_u), however, multiple layers could form due to the continuous supply of buoyancy over the whole box height. By assuming that these layers have the same depth, h, the number of interfaces n was acquired in Cooper & Hunt (2010) by solving

$$\frac{5}{4}\left(\frac{4}{3}\right)^3\left(\frac{A}{\alpha H}\right)^2 = \frac{1}{n(n+1)^3}, \tag{1.1}$$

where the effective area (per unit length) of the box openings is

$$A = 2^{1/2} c_u c_l a_u a_l [(c_u a_u)^2 + (c_l a_l)^2]^{-1/2} \tag{1.2}$$

and α denotes the entrainment coefficient of the wall plume. In (1.2), the dimensionless coefficients c_u and c_l account for the pressure loss at the upper and lower openings, respectively. The buoyancy jump across each density interface was then determined by calculating the increase of buoyancy along the wall plume within a layer over the depth h. Caudwell, Flór & Negretti (2016) considered the case of a thermally heated wall in a sealed box, extending the constant-buoyancy-flux wall-plume analysis of Cooper & Hunt (2010) to a wall of constant temperature. Beyond this knowledge of the stratification and of the associated rate of buoyancy-driven fluid exchange through the openings q_0 ($\mathrm{m^3\ s^{-1}}$), little else was previously known about the flow in the box, including the velocity field and streamline pattern induced by the wall plume within the individual layers.

With the boundary conditions being acquired from the entrainment rate at the plume perimeter, Hunt & Dyke (unpublished observations) deduced a closed-form solution for

the potential flow induced in a ventilated box, with openings at top and base, by a horizontal line source of buoyancy located on its base. Their solution approach was based on the Schwarz–Christoffel transformation which mapped each rectangular layer of the stratification into an upper half-plane. The present paper carries forward their idea by applying this methodology to the more complex stratification produced by a plane vertically distributed buoyancy source.

Beyond solving for the flow pattern in such an emptying–filling box, a further contribution of the present work is to relax a crucial assumption that underlies (1.1), namely, that all layers are of equal depth. It can be readily justified that for a stratification of $n + 1$ layers, n lower layers have the same depth since the volume flow rate of the wall plume in each always increases from zero to the ventilation rate q_0 ($\mathrm{m}^3\ \mathrm{s}^{-1}$). However, inasmuch as the wall plume in the uppermost layer, i.e. the $(n + 1)$th layer, has the distinct behaviour of impinging with and spreading laterally along the ceiling, the depth of this layer cannot be determined straightforwardly. To close their formulation, Linden *et al.* (1990) and Cooper & Hunt (2010) assumed that the uppermost layer had the same depth as the layers below. Analysing the stratification without the above assumption is one of the key goals of the present paper.

In controlled laboratory experiments, releases of saline solution are routinely used as the buoyancy source in a freshwater ambient and it is worth mentioning that with such a vertically distributed buoyancy source of either a planar or a line geometry, the number of layers has never been reported to exceed three (Linden *et al.* 1990; Cooper & Hunt 2010; Gladstone & Woods 2014). Instead, below the freshwater–saline interface, Linden *et al.* (1990) and Cooper & Hunt (2010) described a stably stratified region with alternating high and low buoyancy gradients, whereas Gladstone & Woods (2014) reported a region of near-constant gradient, i.e. of linearly varying density. Gladstone & Woods (2014) adopted a long thin vertical cylinder as their buoyancy source and this distinction of geometry with the planar source makes like-for-like comparisons between the results questionable. As Linden *et al.* (1990) and Cooper & Hunt (2010) pointed out, factors such as vertical mixing and instability may cause a deviation from the theoretically predicted state of multiple ($n > 2$) layers. In addition to there being fewer layers than predicted by the classic model, a characteristic we offer insight into based on a revised model for the stratification (§ 6), it would appear that these layers are generally not as sharp as those achieved with a localised point source producing a classic turbulent plume. Gladstone & Woods (2014) and, more recently, Bonnebaigt, Caulfield & Linden (2018) proposed different models to account for the stably stratified region, both hypothesising that the wall plume detrains continually over its height. Despite the debate above, we retain some aspects of the classic model of multiple layers by Linden *et al.* (1990) to derive the induced flow solution (before deriving a refined form for the stratification and the associated induced flow). This is firstly because, if the actual stratification is regarded as a deviation from the multiple-layer state (predicted by (1.1) for equal-depth layers or by our revised model in § 6), the induced flow derived according to the classic model of stratification is expected to approximate the real flow. Secondly, within each homogeneous layer, the induced flow is potential and can be solved for conveniently, which is beneficial for practical application.

The remainder of this paper is organised as follows. In § 2 the main results of the classic stratification induced by a plane vertically distributed buoyancy source are briefly reviewed. In § 3 the boundary conditions for the induced flow problem are determined by obtaining the entrainment rate along the wall plume. The streamline pattern is then derived in § 4 via conformal mapping techniques. Following a discussion in § 5 on the actual flow expected near the ceiling, in § 6, the near-wall flow in the uppermost layer is analysed by considering both the vertical sidewall plume and horizontal ceiling jet components.

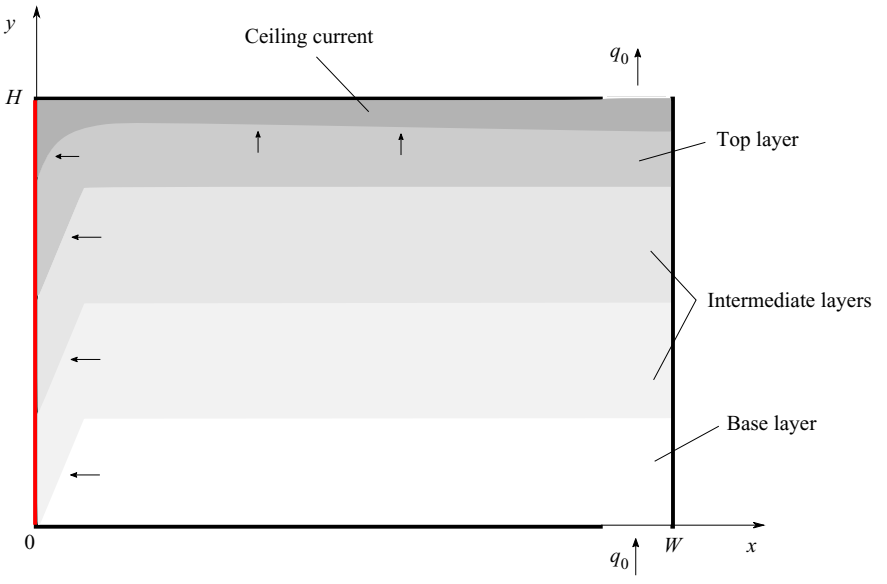

Figure 1. Schematic showing a vertical section through a box with height H and width W, coordinate system and stable stratification established by a turbulent wall plume from a vertically distributed buoyancy source on the wall (left). The stratification induces a volume flow rate q_0 through openings in the base and top. The darkening grey scale indicates regions of increasing buoyancy.

A consequence of this analysis is that the multiple layers do not necessarily have equal depth. In § 7, the streamfunction for the stratification with a ceiling jet is deduced, followed by a discussion on the patterns and controlling parameters. This solution is then extended to arbitrary locations of openings with finite widths. Finally, conclusions are drawn in § 8 where we focus on implications to room ventilation.

2. Wall plume and stratification

Consider a volume of incompressible fluid within a box of horizontal dimensions $W \times L$ and height H, with rectangular openings at the upper and lower corners, as shown in figure 1. The upper and lower openings connect the interior of the box to a quiescent exterior environment of uniform density ρ_0. The left wall of the box emits a constant buoyancy flux per unit area χ ($\mathrm{m}^2\ \mathrm{s}^{-3}$) towards the interior. The dimension L, normal to the page in figure 1, is assumed to be sufficiently large that the time-averaged turbulent convection can be considered as two-dimensional. The flow variables are referred to hereafter with the adjective 'time-averaged' omitted for convenience. The developments that follow assume that a displacement flow is established, i.e. unidirectional outflow at the top opening and inflow at the base opening without interfacial mixing. Hunt & Coffey (2010) establish the critical Froude number at the horizontal plane of the outflow opening that corresponds to transition from unidirectional to bidirectional flow (see also Wise & Hunt 2020) and the maximum Froude number at the inflow opening for which mixing on the interface by the inflow can be considered to be negligible, and thereby identify constraints on the openings and room geometry for which displacement flow is possible. In practical terms, these constraints manifest as lower opening areas that exceed (by a factor of three or greater) upper opening areas and for the turbulent plume that forms from the outflow to be forced or pure, rather than lazy.

Denoting y as the vertical coordinate with origin at the base of the wall, a thin buoyant layer or plume with width $b(y)$ will form and rise against the left wall. In the application of primary interest, namely, to the buoyancy-induced flow in a room, such a wall plume is expected to be turbulent except for the small laminar segment near the base of the wall (Heiselberg & Sandberg 1990; Linden 1999). This plume entrains the ambient fluid through the turbulent eddying motions at its perimeter. We focus exclusively on Boussinesq plumes wherein the density change is so slight that its only significant effect is to modify the body force term in the vertical momentum equation into $g' = g(\rho_e - \rho)/\rho_0$, where ρ and ρ_e denote the local density in the plume and environment, respectively, and g is the acceleration due to gravity. Hereafter g' is referred to as the buoyancy of the plume. Similarly, we define the buoyancy of the environment external to the plume as $g'_e = g(\rho_0 - \rho_e)/\rho_0$.

Following the classic turbulent plume model of Morton, Taylor & Turner (1956), for simplicity 'top-hat' profiles are adopted to approximate the vertical velocity and buoyancy distributions across the plume. In this model, the entrainment velocity U_e, representing the horizontal velocity of fluid entrained into the plume, is assumed to be proportional to the vertical plume velocity v at the same height, i.e.

$$U_e = \alpha v, \tag{2.1}$$

where the entrainment coefficient for a wall plume is chosen to be $\alpha = 0.025$. This value is the midpoint of the range $\alpha \in [0.02, 0.03]$ proposed by Cooper & Hunt (2010) based on experimental measurements. With the molecular diffusion, turbulent transport and wall shear stress neglected, the integral mass, momentum and buoyancy balances for the plume cross-sections are

$$\frac{\mathrm{d}bv}{\mathrm{d}y} = \alpha v, \quad \frac{\mathrm{d}bv^2}{\mathrm{d}y} = bg', \quad \frac{\mathrm{d}bvg'}{\mathrm{d}y} = \frac{bvg}{\rho_0}\frac{\mathrm{d}\rho_e}{\mathrm{d}y} + \chi, \tag{2.2a–c}$$

cf. Cooper & Hunt (2010). While Kaye & Cooper (2018) show how the wall shear stress modifies the profiles across the plume, our focus herein is on the development of a first-order model for the induced flow. As such, we make the simplification of neglecting the shear stress. Based on the modelling framework we develop (§§ 2 and 3), wall shear stress could be readily incorporated at a later stage.

According to Linden *et al.* (1990) and Cooper & Hunt (2010), n horizontal density interfaces will form in the steady state, with the relationship between n and the dimensionless effective area given by (1.1). The wall plume within each layer rises and horizontally intrudes to form the layer above, where a new wall plume generates and develops in the same manner. This gives rise to the stable layered stratification depicted in figure 1. Thus, the conservation relations (2.2*a–c*) can be applied to the wall plume in any layer to solve for the plume velocity and buoyancy variations with height as well as the buoyancy of the layers. Since the plume volume flux in each layer, except for the uppermost, always increases from zero to the ventilation flow rate, q_0, all n lower layers must have an identical depth, h_0. The depth h_1 of the top layer may be different, as we explore in §§ 5 and 6, and is related to h_0 as follows

$$h_1 = H - nh_0. \tag{2.3}$$

Linden *et al.* (1990) and Cooper & Hunt (2010) both assumed

$$h_1 = h_0, \tag{2.4}$$

which predicted multiple layers, all of equal depth. However, in the three-layer stratification observed in Cooper & Hunt (2010), their figure 6, while the two lower layers

are of similar depth, the top layer is considerably thinner. In the present work, this classic model of stratification will be adopted, at first to derive the induced flow field and then a refined model for the stratification.

2.1. *Non-dimensionalisation*

To proceed, we non-dimensionalise (2.2*a–c*) based on the scalings

$$\left.\begin{gathered} q = bv = \alpha^{2/3} H^{4/3} \chi^{1/3} q^*, \quad m = bv^2 = \alpha^{1/3} H^{5/3} \chi^{2/3} m^*, \\ f = bvg' = H\chi f^*, \quad y = Hy^*, \end{gathered}\right\} \tag{2.5a–d}$$

where q, m and f represent the specific mass, momentum and buoyancy fluxes, respectively, and the starred variables their dimensionless counterparts. The corresponding characteristic velocity and buoyancy scales are therefore $\alpha^{-1/3} H^{1/3} \chi^{1/3}$ and $\alpha^{-2/3} H^{-1/3} \chi^{2/3}$. Finally, the dimensionless width of the box, denoted as $2a = W/H$, is equivalent to the box aspect ratio, $\mathcal{A}$.

Hereafter, all variables are dimensionless unless stated otherwise. With the superscript $(\cdot)^*$ omitted for convenience, the dimensionless conservation equations for the wall plume are

$$\frac{\mathrm{d}q}{\mathrm{d}y} = \frac{m}{q}, \quad \frac{\mathrm{d}m}{\mathrm{d}y} = \frac{qf}{m}, \quad \frac{\mathrm{d}f}{\mathrm{d}y} = 1. \tag{2.6a–c}$$

For the source conditions $q = m = f = 0$ at $y = (j-1)h_0$ (counting from the base layer where $j = 1$), the solution of (2.6*a–c*) for the jth layer is

$$\left.\begin{gathered} q = c_1 [y - (j-1)h_0]^{4/3}, \quad m = \tfrac{4}{3} c_1^2 [y - (j-1)h_0]^{5/3}, \\ f = y - (j-1)h_0, \quad b = \tfrac{3}{4}\alpha [y - (j-1)h_0], \end{gathered}\right\} \tag{2.7a–d}$$

where $c_1 = 3\sqrt[3]{100}/20 \approx 0.70$ to two significant figures (2 s.f.). Details of the solution of (2.6*a–c*) that leads to (2.7*a–d*) can be found in Cooper & Hunt (2010). Since conservation of volume requires q_0 to be equal to the dimensionless volume flux across any horizontal section of the box, q_0 can be acquired by calculating the plume volume flux at an interface height. Thus,

$$q_0 = q(h_0) = c_1 h_0^{4/3}, \tag{2.8}$$

where the depth of each of the $(n+1)$ layers

$$h_0 = 1/(n+1), \tag{2.9}$$

is yet to be determined. The number of interfaces n can be calculated by combining (2.8) with the relationship

$$q_0 = \frac{A}{\alpha H} \left(\int_0^1 g'_e \, \mathrm{d}y \right)^{1/2} = \frac{h_0^{1/2} A}{\alpha H} \left(\sum_{j=1}^{n+1} g'_{e,j} \right)^{1/2}, \tag{2.10}$$

where A and H have dimensions of length, and $g'_{e,j}$ denotes the buoyancy in the jth layer. Details on the derivation of (2.10) are given, for example, in Linden *et al.* (1990) who assume that Bernoulli's principle is valid inside and outside the box. While we prescribe $g'_{e,1} = 0$ as the buoyancy of the base layer, the layer buoyancy increases upwards with a

common difference of $g'(h_0)$ between successive layers. Since, from (2.7*a–d*), the plume buoyancy is

$$g' = f/q = c_1^{-1}[y - (j-1)h_0]^{-1/3}, \tag{2.11}$$

the buoyancy of the layers must follow

$$g'_{e,j} = (j-1)c_1^{-1}h_0^{-1/3} \quad j = 1, \ldots, n+1. \tag{2.12}$$

By substituting (2.8) and (2.12) into (2.10), the relation (1.1) determining the stratification in Cooper & Hunt (2010) is recovered. With n known, the ventilation flow rate is then determined by substituting h_0 from (2.9) into (2.8).

By differentiating the plume volume flux in (2.7*a–d*) with respect to height, the entrainment rate in the jth layer is determined as

$$U_e = \frac{\mathrm{d}q}{\mathrm{d}y} = \frac{4}{3}c_1[y - (j-1)h_0]^{1/3}, \tag{2.13}$$

which leads to the boundary condition for the induced flow at the left boundary.

3. Formulation for the induced flow

Following the classic assumption, the flow induced by the plume motion is treated as a potential flow (e.g. Taylor 1958; Kotsovinos 1977; Yih 1980). Whilst this assumption is weakest near the plume perimeter, a wall or an interface (see § 7.6) where there may be a strong shear, in the bulk of the box interior where velocity gradients are anticipated to be weak, this well-proven approximation is expected to provide an appropriate model for the flow. Each layer, with dimensions $h \times 2a$ (h being either h_0 or h_1), will be considered in turn after applying the coordinate translation $(x_j, y_j) = (x - a, y - (j-1)h_0)$ which shifts the j_{th} layer to the centred location, as shown in the left-hand side of figure 2. In the following analysis, the subscript $(\cdot)_j$ is omitted for convenience. Within each rectangular layer, the streamfunction satisfies the Laplace equation

$$\nabla^2\psi = 0, \tag{3.1}$$

where ψ scales with $\alpha^{-1/3}H^{4/3}\chi^{1/3}$. The plume against the left wall (figure 1) is treated as a single-sided 'sink line' which captures the effect of entrainment on the induced flow, and is approximated as being distributed along the wall since the wall plume is very thin. The strength of the sink sheet, $\Gamma(y) = \mathrm{d}\psi/\mathrm{d}y$, that quantifies the volume flux into the wall plume, must be equal to the entrainment rate. Hence,

$$\frac{\mathrm{d}\psi}{\mathrm{d}y} = -U_e, \tag{3.2}$$

which, on referring to (2.13), indicates that at the left boundary of the j_{th} layer

$$\psi = \psi_0 - c_1 y^{4/3}, \tag{3.3}$$

where ψ_0 denotes the value of the streamfunction at the base of the wall plume in this layer. Also, on account of the no-penetration condition at the walls and across the interfaces, the streamfunction is constant along such boundaries, except where it changes abruptly owing to inflow, either from the exterior or the wall plume in the layer below.

Since all intermediate layers are identical according to the description of the stratification in § 2, there are three types of layer: base, intermediate and top.

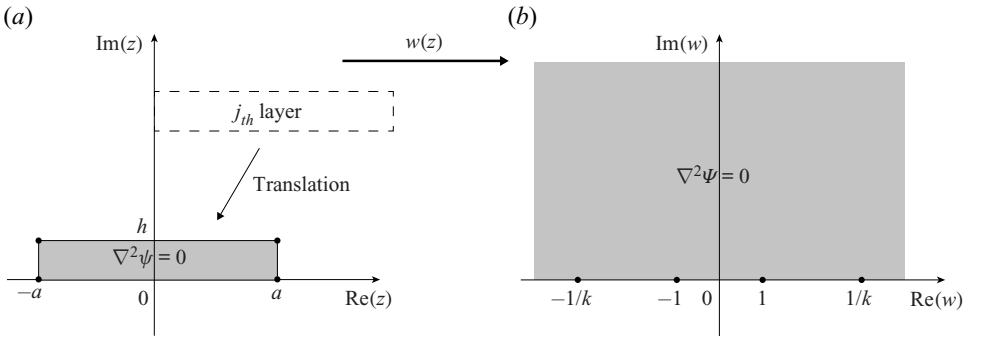

Figure 2. The translation of the j_{th} layer to the centred location (a) and the conformal mapping of this layer, under the mapping $w = \mathrm{sn}(z/C; k)$, to the upper half-plane (b).

Furthermore, to be compatible with the classic assumption of equal-depth layers, it is proposed that once the wall plume turns through a right angle to form a horizontal current at the ceiling, it flows towards the upper opening without any fluid exchange with the ambient. Thus, the depth of the top layer must be identical to the other layers in order that the volume flow rate of the ceiling current be equal to the ventilation flow rate. With the streamfunction also being constant along the upper boundary, the top layer has the same boundary conditions as the intermediate layers.

Assuming, without loss of generality, $\psi = 0$ along the base of the box, the induced flow in the base layer must satisfy the boundary conditions

$$\left.\begin{array}{cc} \psi = -c_1 y^{4/3} & \text{on } x = -a \;\&\; 0 \leqslant y \leqslant h \\ \psi = 0 & \text{on } -a \leqslant x \leqslant a \;\&\; y = 0 \\ \psi = -q_0 & \text{on other boundaries.} \end{array}\right\} \tag{3.4}$$

Similarly, the boundary conditions for any intermediate layer and the top layer are

$$\left.\begin{array}{cc} \psi = -c_1 y^{4/3} & \text{on } x = -a \;\&\; 0 \leqslant y \leqslant h \\ \psi = -q_0 & \text{on other boundaries,} \end{array}\right\} \tag{3.5}$$

where the lower-left corner is thereby treated as a potential flow point source of strength q_0.

4. Solution via conformal mapping

To acquire the streamline pattern for the induced flow, it will simplify the problem significantly to map the rectangular domain of each layer to an upper half-plane, as illustrated in figure 2, as Poisson's integral formula immediately provides us with the solution in the half-plane. With $z = x + \mathrm{i}y$ denoting the original complex plane, where $i = \sqrt{-1}$, the inverse mapping from the upper half-w-plane, where $w = u + \mathrm{i}v$, to the z-plane, as a special case of the Schwarz–Christoffel transformation, is

$$z = C \int_0^w \frac{1}{(1 - t^2)^{1/2}(1 - k^2 t^2)^{1/2}}\, \mathrm{d}t. \tag{4.1}$$

Taking the inverse of (4.1), the conformal mapping to the upper half-plane is $w = \mathrm{sn}(z/C; k)$, where sn is the Jacobian elliptic sine function with modulus k. The four vertices

of the rectangle are mapped in such a way that $-a+\mathrm{i}h \mapsto -1/k$, $-a \mapsto -1$, $a \mapsto 1$ and $a+\mathrm{i}h \mapsto 1/k$ (Driscoll & Trefethen 2002, chapter 2). According to the correspondences of the vertices, k and the coefficient C can be determined from

$$a/C = \mathrm{sn}^{-1}(1;k) \quad \text{and} \quad (a+\mathrm{i}h)/C = \mathrm{sn}^{-1}(1/k;k), \tag{4.2a,b}$$

which implies

$$\frac{h}{a} = \frac{K(\sqrt{1-k^2})}{K(k)} \quad \text{and} \quad C = \frac{a}{K(k)}, \quad \text{where } K(k) = \int_0^1 \frac{1}{\sqrt{(1-t^2)(1-k^2t^2)}}\,\mathrm{d}t \tag{4.3}$$

is the complete elliptic integral of the first kind. For a given layer aspect ratio $h/(2a)$, k is solved for using the bisection method, after which C is determined. With $\Psi(w)$ denoting the streamfunction on the w-plane, from the standard result $\nabla_z^2\psi = D(z)\nabla_w^2\Psi$ (Driscoll & Trefethen 2002), where $D(z) = |\mathrm{d}\,\mathrm{sn}(z)/\mathrm{d}z|^2 \neq 0$, it is deduced that $\nabla_w^2\Psi = 0$ in the upper half of the w-plane. Thus, the form of governing equation for the streamfunction is unchanged through the mapping.

The boundary conditions change accordingly through the mapping. On the mapped boundary, i.e. the real axis of the w-plane, they become

$$\Psi(u,0) = \begin{cases} -q_0 & u < -\dfrac{1}{k} \\ -c_1[-\mathrm{i}(C\,\mathrm{sn}^{-1}(u)+a)]^{4/3} & -\dfrac{1}{k} \leqslant u < -1 \\ 0 & -1 \leqslant u < 1 \\ -q_0 & u \geqslant 1, \end{cases} \tag{4.4}$$

for the base layer, and for every other layer

$$\Psi(u,0) = \begin{cases} -q_0 & u < -\dfrac{1}{k} \\ -c_1[-\mathrm{i}(C\,\mathrm{sn}^{-1}(u)+a)]^{4/3} & -\dfrac{1}{k} \leqslant u < -1 \\ -q_0 & u \geqslant -1. \end{cases} \tag{4.5}$$

With the boundary conditions along the real axis known, Ψ is given by the Poisson integral formula

$$\Psi(u,v) = \frac{v}{\pi}\int_{-\infty}^{+\infty} \frac{\Psi(\xi,0)}{(\xi-u)^2+v^2}\,\mathrm{d}\xi. \tag{4.6}$$

Hence,

$$\Psi(u,v) = \frac{v}{\pi}\left(\int_{-\infty}^{-1/k} F_1\,\mathrm{d}\xi + \int_{-1/k}^{-1} F_2\,\mathrm{d}\xi + \int_{-1}^{1} F_3\,\mathrm{d}\xi + \int_{1}^{1/k} F_4\,\mathrm{d}\xi + \int_{1/k}^{\infty} F_5\,\mathrm{d}\xi\right), \tag{4.7}$$

where the integrand in each term is determined solely by the boundary condition on the corresponding interval, as given in (4.4) and (4.5). Mapped and translated back to the original rectangular domain, the streamfunction in the j_{th} layer is

$$\psi(z) = \Psi\left(\mathrm{sn}\left((z-z_0)/C;k\right)\right), \tag{4.8}$$

where $z_0 = a + i(j-1)h_0$.

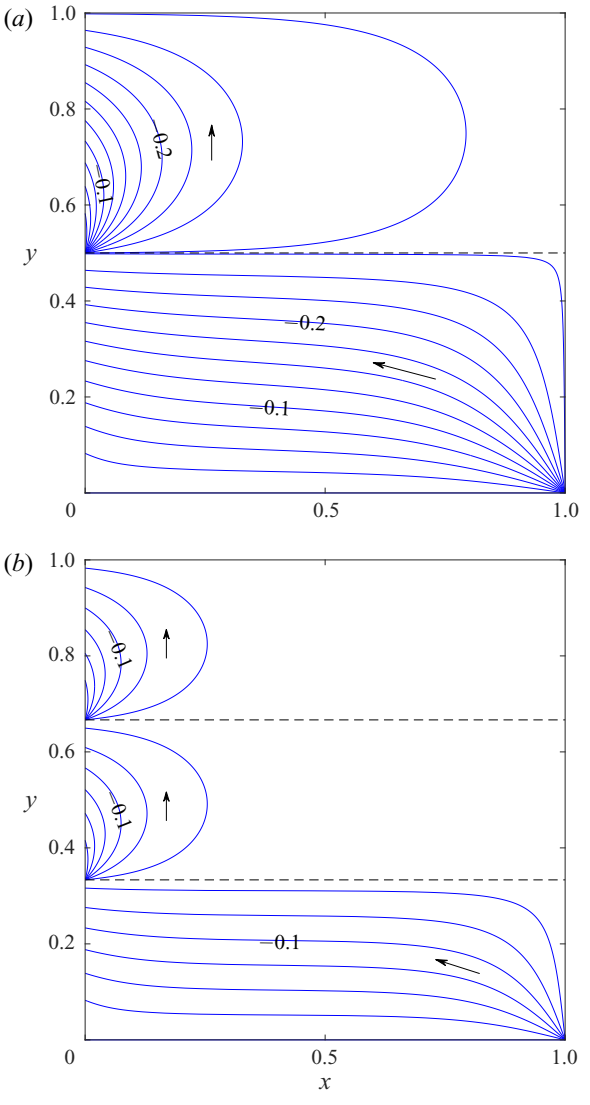

Figure 3. Induced flow patterns driven by a plane vertically distributed buoyancy source in a square emptying–filling box ($\mathcal{A} = 1$) with the classic high- and low-level opening configuration. The equal-layer-depth stratification model of Linden *et al.* (1990) and Cooper & Hunt (2010) is adopted. The step between two adjacent streamlines is $\Delta\psi = 0.025$. Arrows indicate the general direction of flow. Dashed lines indicate interface positions. (*a*) Two-layer stratification, $n = 1$. (*b*) Three-layer stratification, $n = 2$.

4.1. *Flow pattern*

Streamlines for the induced flow solution (4.7) in a square box are plotted in figure 3 for (*a*) two-layer and (*b*) three-layer stratifications. The base layer is characterised by what may be regarded as a 'smooth horizontal flush': fluid entering through the lower opening moves nearly horizontally across the region (from right to left) thereby continuously flushing the layer. On approaching the left-hand wall, the induced flow tilts upwards before being entrained into the wall plume. Meanwhile, common to each layer above is an induced flow motion that is concentrated near the wall, adjacent to which is a region of near-stagnant fluid.

Prior to exploring these flow patterns further, we proceed by questioning and subsequently relaxing the classic assumption of equal-depth layers (2.4). This allows for a refined prediction of the stratification whose induced flow we then evaluate and assess.

5. Ceiling flow regimes

Uncertainty regarding the precise details of the interaction between the wall plume and the ceiling necessitates the introduction of assumptions to model the outflow from the impingement region. The model for the classic stratification (Linden *et al.* 1990) implicitly assumes that, upon impingement with the ceiling (at $y = 1$), the entire body of buoyant fluid transported vertically in the wall plume is turned through a right angle to propagate as a horizontal current without further fluid exchange with the ambient. Although a useful model, the actual flow scenario near the ceiling may be quite different. Indeed, in the flow observations made by Cooper & Hunt (2010), layers of identical depth were not evident as the top layer was markedly thinner.

If one considers where the wall plume impinges with the ceiling, we note that the vertical momentum flux of the plume is reduced to zero and the volume flux transported by the plume provides the 'source' volume flux for the horizontal current. Hunt & Dyke (submitted), who consider the induced flow established by a localised line source at the base of an emptying–filling box, initially proposed to model the outflow from the impingement region into the ambient in two ways: first, in the spirit of a simplified model, as a potential flow source; however, this simplification means that the buoyant outflow need not remain attached to the ceiling as anticipated in practice; and second, as a turbulent ceiling jet, since entrainment can occur across the perimeter of the current if the shear is strong enough to overcome the stable stratification. Herein, we adopt the latter approach.

A final uncertainty we raise concerns the relative strengths of the ceiling current and the draining flow. If, for example, the upper opening area is too small to sustain the entire volume flux of the ceiling current, the excess fluid will impinge on the right-hand wall and potentially drive an overturning motion, as described by Kaye & Hunt (2007) for a current originating from the impingement of a point source plume. Remarkably little is currently known about overturning motions associated with steady flows in ventilated boxes and whilst ventilation flows driven by a range of different plume geometries have been investigated (Linden *et al.* 1990; Cooper & Linden 1996; Linden & Cooper 1996; Hunt & Linden 2001, 2005; Cooper & Hunt 2010), to our knowledge these motions have not been reported in any detail. Moreover, acquiring meaningful experimental results on the ceiling flow scenarios is extremely difficult for a number of reasons. For example, when pumping saline solution through a porous wall to produce the plume in an aqueous environment (cf. Cooper & Hunt 2010; Gladstone & Woods 2014; Bonnebaigt *et al.* 2018) it is nearly impossible to maintain a uniform buoyancy flux. During the course of such an experiment the developing stratification reduces the flux of buoyancy from the wall and so the measurements made at a suitably large time are not those driven by the intended source conditions.

However, among the few, the experiments of Cooper & Hunt (2010) did suggest a representative ceiling flow regime. They observed that the ceiling current was well established without any indication of mixing associated with an energetic impingement at the ceiling, or evidence of overturning at the side wall opposite the plume source. Thus, in the flow regime they observed, the wall plume turned smoothly upon reaching the ceiling and the resulting current drained out totally through the upper opening without inducing an overturning motion.

In the modelling that follows (§ 6) we adopt this description of the flow, wherein we assume that net entrainment is present along the perimeter of the ceiling current. This assumption will be justified in § 7.6 on account of the high shear rate that we deduce from the induced flow solution.

6. Stratification with an entraining ceiling current

As proposed in § 5 and depicted in figure 1, for the top layer of the ceiling flow regime the sum of the volume fluxes entrained horizontally by the wall plume and vertically by the ceiling current over the interval $[0, 2a]$ must be equal to the ventilation flow rate q_0. Defining $q_{ce}(x)$ as the volume flow rate in the ceiling current, we therefore write

$$q_{ce}(x = 2a) = q_0. \tag{6.1}$$

Continuity at the top-left corner requires

$$q_{ce}(x = 0) = q(y = 1), \quad g'_{ce}(x = 0) = g'(y = 1), \quad d_{ce}(x = 0) = b(y = 1), \tag{6.2a–c}$$

where $g'_{ce}(x)$ and $d_{ce}(x)$ denote the reduced gravity and the depth of the ceiling current. Thus, the depth-averaged horizontal velocity of the current $u_{ce}(x) = q_{ce}(x)/d_{ce}(x)$. To establish the dynamical condition of the ceiling current we define the ratio of the inertia and buoyancy forces at its source ($x = 0$) by means of the Froude number

$$Fr_s := \frac{u_{ce}(0)}{\sqrt{g'_{ce}(0)\, d_{ce}(0)}}. \tag{6.3}$$

With reference to (2.7*a–d*), (2.11) and (6.2*a–c*) we have

$$Fr_s = \left(\frac{4c_1}{3\alpha}\right)^{3/2} \approx 226. \tag{6.4}$$

Thus, given $Fr_s \gg 1$ it is reasonable to neglect the role of the buoyancy force in the development of the ceiling current and proceed under the assumption that the dynamical aspects of the current are approximated by those of a horizontal wall jet.

The scalings and empirical relationships of Rajaratnam (1976) for a horizontal plane wall jet enable the local volume flux $q_{ce}(x)$ and depth $d_{ce}(x)$ of the ceiling current to be expressed as

$$q_{ce}(x) = c_2 q_{ce}(0)\sqrt{\frac{x - x_{vs}}{d_{ce}(0)}} \quad \text{and} \quad d_{ce}(x) = c_2^2(x - x_{vs}), \tag{6.5a,b}$$

respectively. In (6.5*a*,*b*), the constant $c_2 = 0.26$ (Rajaratnam 1976) and x_{vs} denotes the virtual source location of the ceiling current. By substituting $x = 0$ into (6.5*a*,*b*), the location of the virtual source is

$$x_{vs} = -\frac{d_{ce}(0)}{c_2^2} = -\frac{3\alpha h_1}{4c_2^2}. \tag{6.6}$$

Substituting for (2.8) and (6.5*a*,*b*) into (6.1), and recalling that $h_1 = 1 - nh_0$, yields

$$(1 - nh_0)^{8/3} + \left(4c_2^2 a/(3\alpha)\right)(1 - nh_0)^{5/3} - h_0^{8/3} = 0. \tag{6.7}$$

Re-deriving (2.10) without making the assumption of equal-depth layers gives

$$q_0 = \frac{A}{\alpha H}\left(\int_0^1 g'_e \,\mathrm{d}y\right)^{1/2} = \frac{A}{\alpha H}\left(\sum_{j=1}^{n} g'_{e,j} h_0 + g'_{e,n+1} h_1\right)^{1/2}. \tag{6.8}$$

Substituting for (2.8) and (2.12) into (6.8) leads to the following cubic in h_0:

$$2c_1^3\alpha^2\,(H/A)^2\,h_0^3 + (n^2+n)h_0 - 2n = 0. \tag{6.9}$$

To proceed, we note that on specifying n and $a = W/(2H)$, the two equations (6.7) and (6.9) form a closed system for the two unknowns h_0 and A/H.

At this stage it is useful to highlight some key distinctions between the classic model (1.1) and the approach taken herein. Distinct from other emptying–filling-box flows, whose steady states do not exhibit a dependence on the lateral dimension of the box (e.g. Linden *et al.* 1990; Linden & Cooper 1996; Gladstone & Woods 2001; Hunt & Linden 2001, 2005), (6.7) clearly indicates such a dependence. Additionally, (1.1) only permits solutions for A/H that correspond to integer values of n. Our model overcomes this limitation given that a range of different $\{A/H, a\}$ corresponds to a given n on account that the layer depths adjust due to entrainment by the ceiling current.

6.1. *Predictions of layer depth and constraints on model*

Before solving for the induced flow, it is informative to examine the refined stratification pattern and assess how it differs from the equal-depth-layer stratification. Figure 4 shows the correspondence between the number of layers n in a box with aspect ratio $\mathcal{A} = W/H$ and effective area A/H. A point of note is that A/H cannot be prescribed *a priori*, but rather there is a unique value of A/H that corresponds to a given number of interfaces for a box of aspect ratio $\mathcal{A}$. From a practical perspective, e.g. in a ventilated room, A/H cannot be specified precisely, even if a_l, a_u and H can be. The underlying reason for this is that the discharge coefficient associated with the upper opening, c_u in (1.2), has been shown by Hunt & Holford (2000) and Holford & Hunt (2001) to depend on the local Richardson number for flow through that opening – a quantity whose value is not known at the outset and would require a complex set of measurements in order to estimate. Moreover, on activating the wall plume, the value of c_u will continuously adjust as the flow develops toward a steady state until $(\mathcal{A}, A/H)$ falls onto a nearby contour of $n =$ constant (figure 4); c_l will also adjust as the Reynolds number of the flow through the lower opening increases (Ward-Smith 1980). While for $n > 2$ the stratification is insensitive to the box aspect ratio, decreasing the effective opening area A/H tends to increase the number of layers. To achieve at least three layers requires $A/H < 0.007$. Moreover, as the number of layers increases, the incremental reduction in A/H that gives rise to an additional layer becomes increasingly small (figure 4).

Figure 5 illustrates how the layer depths, h_1 (top layer) and h_0 (lower layers), vary with n in a square box. The predictions of our model are shown (h_1 solid line, h_0 dot-dashed line) together with those of Linden *et al.* (1990) (dashed line). The depth of the lower layer we predict is greater than that predicted in Linden *et al.* (1990) and the difference decreases with n. Evidently, the top layer is significantly thinner than the lower layers and thins on increasing n. The prediction of a markedly thinner top layer in this refined stratification model aligns well with the observations in Cooper & Hunt (2010). Our model predicts that $h_1 \to 0$ as $n \to \infty$. As such, for sufficiently large n, the top layer would only marginally exceed the depth of the ceiling current, turbulent entrainment into which

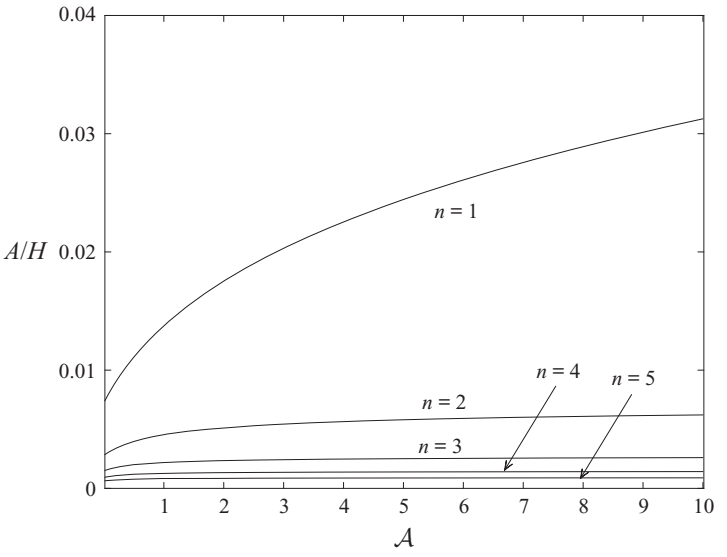

Figure 4. Plot of the solution of (6.7) and (6.9) showing the correspondence between the number of layers n with aspect ratio $\mathcal{A}$ and effective area A/H.

could then erode the interface in practice. In such a case, our model breaks down and the potential coalescence of layers may offer a reason as to why the number of layers observed in experiments is limited to just a few. Insisting $d_{ce}(1) \ll h_1$, with reference to (6.5*a*,*b*), we obtain the following constraint:

$$h_1(\mathcal{A}=1) \gg \frac{c_2^2}{1-3\alpha/4} \approx 0.07. \tag{6.10}$$

Equivalently, an upper bound on the aspect ratio, $\mathcal{A} = \mathcal{A}_{max}$, for which our model is valid may be acquired on letting $d_{ce}(\mathcal{A}_{max}) = h_1$ in (6.5*a*,*b*), from which

$$\mathcal{A}_{max} = h_1 \left(\frac{1-3\alpha/4}{c_2^2} \right). \tag{6.11}$$

Substituting this and $a = \mathcal{A}_{max}/2$ into (6.7), we obtain $\mathcal{A}_{max}(n=1) = 3.25$ for a two-layer stratification and $\mathcal{A}_{max}(n=2) = 1.83$ for a three-layer stratification.

For a square box ($\mathcal{A}=1$), the constraint $h_1(\mathcal{A}=1) \gg 0.07$ (6.10) restricts the number of interfaces to no more than three (see h_1-curve in figure 5*a*). Cooper & Hunt (2010) used a box with dimensions 60 cm × 41.2 cm × 15 cm ($W \times H \times L$) giving $\mathcal{A} = 1.46$. For this geometry we require $h_1(\mathcal{A}=1.46) \gg 0.10$ which, with reference to figure 5(*b*), indicates that at most two interfaces should be possible – this is indeed what Cooper & Hunt (2010) observed.

7. Induced flow pattern

7.1. *Solution for the refined stratification*

The approach developed in §§ 2–4 remains valid for the new model of stratification (§ 6), but the boundary conditions for the top layer developed earlier need to be modified.

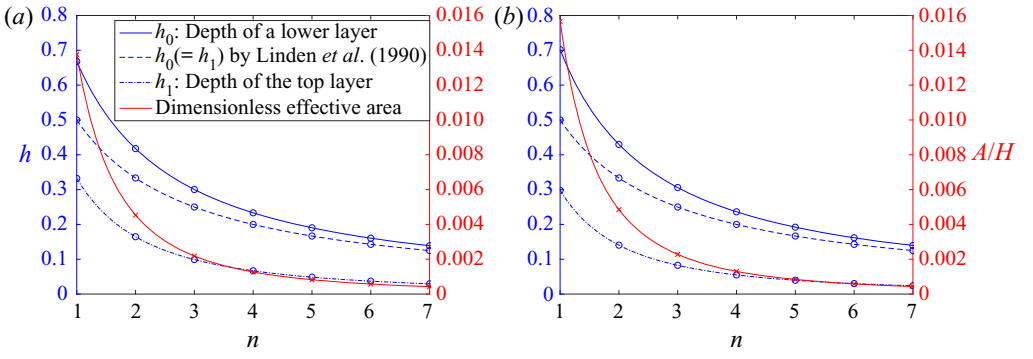

Figure 5. The reduction in the dimensionless layer depth with the number of interfaces. The depths of lower layers h_0 and top layer h_1 are plotted from the solution of (6.7) and (6.9). The Linden *et al.* (1990) prediction, (1.1), is displayed for comparison. The red line, with scale given on the right-hand side vertical axis, plots the variation of A/H with n: (*a*) $\mathcal{A} = 1$; (*b*) $\mathcal{A} = 1.46$, the aspect ratio used in the experiments of Cooper & Hunt (2010).

Since the gradient of the streamfunction along the upper boundary is equal to the entrainment flux of the ceiling current, the boundary conditions for the top layer are

$$\left.\begin{array}{ll} \psi = -c_1 y^{4/3} & \text{on } x = -a \;\&\; 0 \leqslant y \leqslant h_1 \\ \psi = -c_1 c_2 h_1^{4/3} \sqrt{\dfrac{2(x+a)}{3\alpha h_1} + \dfrac{1}{c_2^2}} & \text{on } -a \leqslant x \leqslant a \;\&\; y = h_1 \\ \psi = -q_0 & \text{on other boundaries.} \end{array}\right\} \tag{7.1}$$

On applying the conformal mapping (4.1), the physical boundaries map to the real axis of the w-plane with the following boundary conditions

$$\Psi = \left\{\begin{array}{ll} -c_1 c_2 h_1^{4/3} \sqrt{\dfrac{2(C\,\mathrm{sn}^{-1}(u) + a - \mathrm{i}h_1)}{3\alpha h_1} + \dfrac{1}{c_2^2}} & u < -\dfrac{1}{k} \\ -c_1[-\mathrm{i}(C\,\mathrm{sn}^{-1}(u) + a)]^{4/3} & -\dfrac{1}{k} \leqslant u < -1 \\ -q_0 & -1 \leqslant u < 1/k \\ -c_1 c_2 h_1^{4/3} \sqrt{\dfrac{2(C\,\mathrm{sn}^{-1}(u) + a - \mathrm{i}h_1)}{3\alpha h_1} + \dfrac{1}{c_2^2}} & u \geqslant 1/k. \end{array}\right\} \tag{7.2}$$

Substitution of (7.2) into (4.7) yields the solution for the induced flow in the top layer. Although now of an increased height, the solution for the flow in any of the lower layers is unchanged from that developed in § 4. The induced flow solution for the stratification in a square box with ceiling current is plotted in figures 6(*a*)–6(*c*) for $n = 1$, 2 and 3, respectively.

7.2. *General flow pattern*

A first point of note is that the general pattern of flow in each type of layer, types which we shall refer to as the top, intermediate and base layers, remains unchanged regardless of the number of interfaces n (figure 6). To assist the following discussion, the distribution of

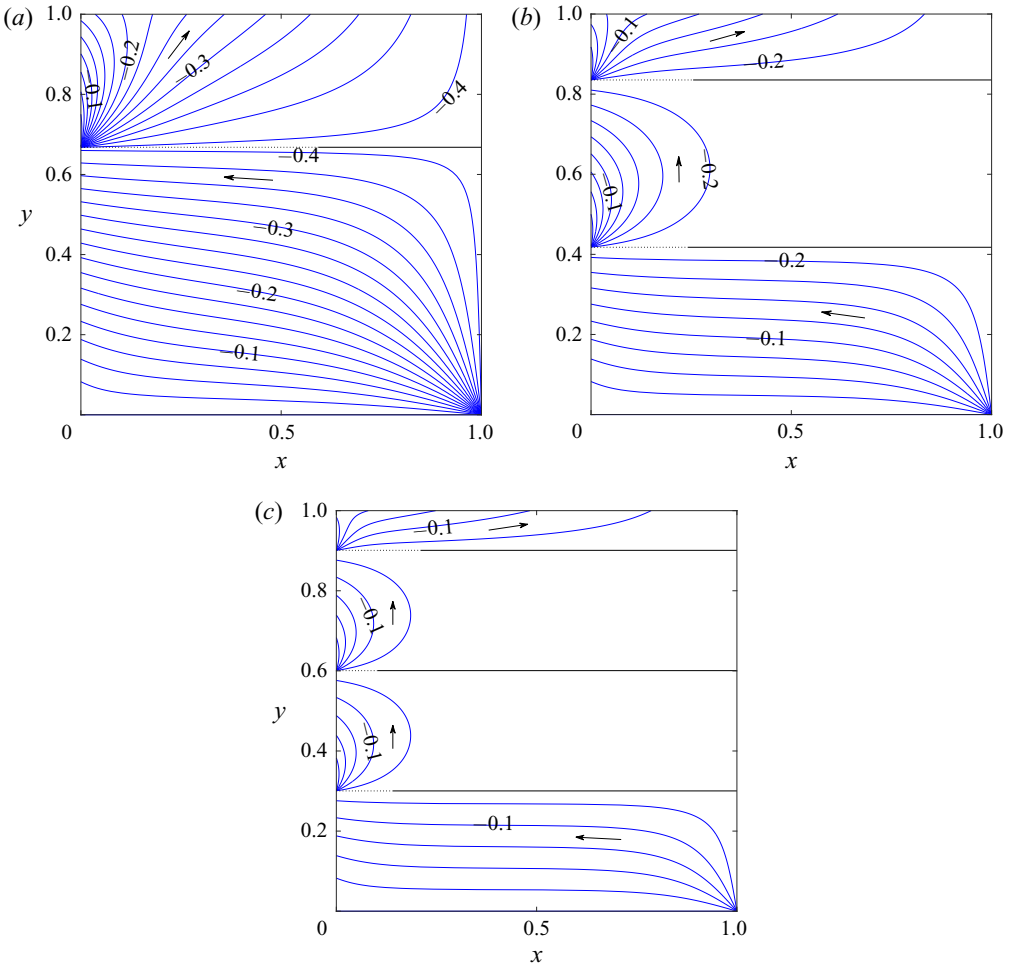

Figure 6. Induced flow patterns in a square emptying–filling box ($\mathcal{A} = 1$) driven by a plane vertically distributed buoyancy source with ceiling current; (*a*) $n = 1$, (*b*) $n = 2$, (*c*) $n = 3$. The step between adjacent streamlines is $\Delta\psi = 0.025$. Arrows indicate the general direction of flow. The position of each interface is shown as a horizontal line; the solid part of the line represents where the interface is predicted to be linearly stable (and the dotted part, unstable) based on the simplified analysis of § 7.6.

dimensionless flow velocity magnitude $U(x, y)$ for the three-layer case, corresponding to the streamline plot figure 6(*b*), is plotted in figure 7.

Entering through the lower opening at ($x = 1, y = 0$), the flow turns smoothly and is drawn near horizontally towards the buoyancy source (left wall, y-axis). Interestingly, the streamlines tend to tilt upwards at the left wall in response to the wall-plume entrainment. Evidently, the flow in the upper-right region of the base layer is relatively slow (figure 7*c*).

The flow in the bulk of the intermediate layer (figure 6*b*), or intermediate layers (figure 6*c*), is near stationary. The majority of the motion is confined to the region adjacent to the left wall. This motion is created as buoyant fluid, discharged into an intermediate layer from the outflow of the wall plume below, is re-entrained into the wall plume of the intermediate layer. The existence of the large-scale quiescent region (figure 7*b*) implies that, for the application of room ventilation, the air is stale at middle heights. As highlighted in appendix A, correctly locating the lower opening is crucial to avoid

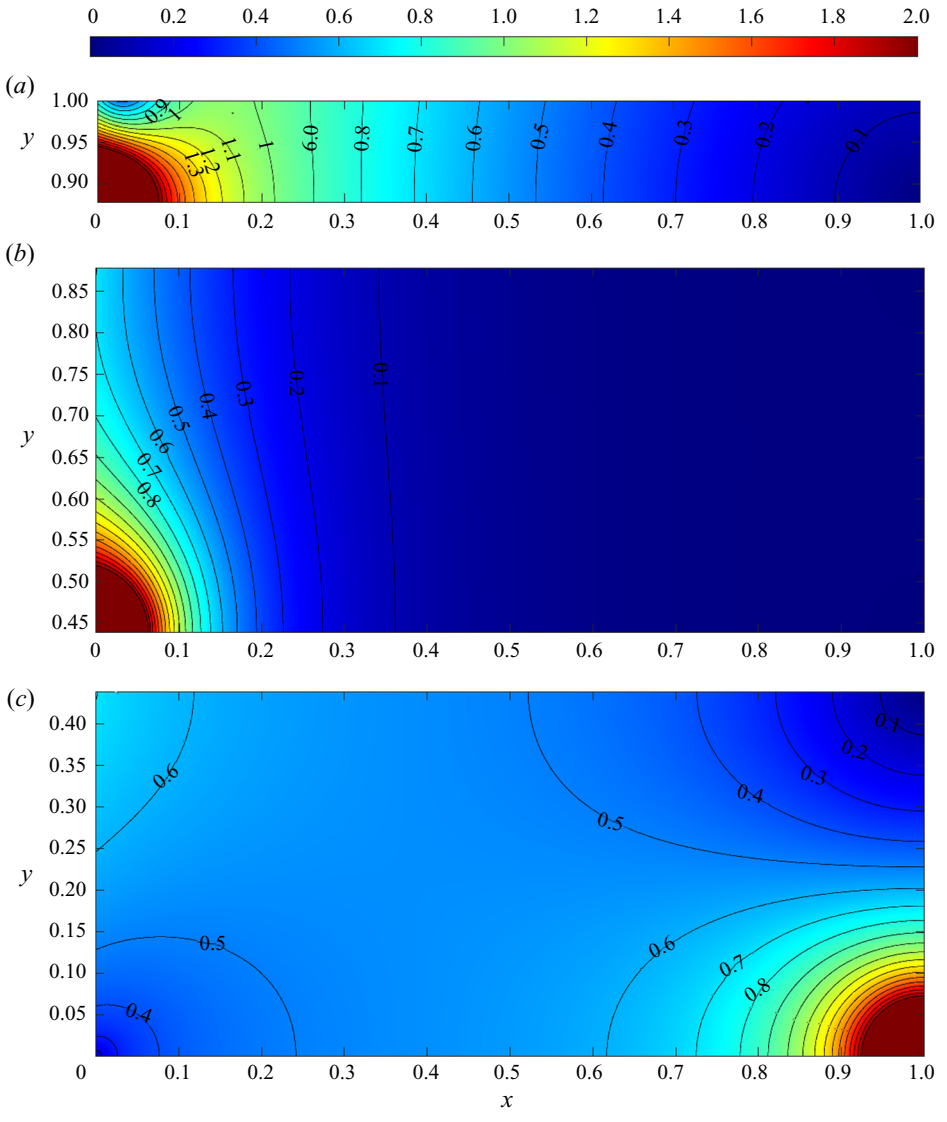

Figure 7. Colour map and contours showing the distribution of dimensionless velocity magnitude $U(x, y)$ corresponding to the streamline pattern for $\mathcal{A} = 1$ and $n = 2$ shown in figure 6(*b*). (*a*) Top layer. (*b*) Intermediate layer. (*c*) Base layer. The velocity associated with each colour is indicated on the horizontal scale above (*a*).

similar large-scale regions of stale air within the base layer. Designers should ensure that the stale region is above the height, H_l (m), of the living zone. The corresponding design criterion is $h_0(n, \mathcal{A}) > H_l/H$.

The streamline pattern in the top layer is most easily appreciated in figure 6(*a*). Immediately above the interface and adjacent to the wall plume, the flow pattern is similar to that in any intermediate layer. While a portion of the volume flux supplied to the top layer from below is transported by entrainment towards the left wall, the bulk forms the ceiling current. The region near the upper opening (at $x = 1$, $y = 1$) is relatively quiescent, cf. figure 7(*a*).

7.3. *Velocity magnitude distribution*

With reference to figure 7, the velocity magnitude U within each layer is the highest at the region of inflow, and gradually decays away from this region. In the base layer, the velocity magnitude in the central region is between $U = 0.5$ and $U = 0.6$, and relatively uniform; elsewhere, U tends to increase towards the upper-left and lower-right corners, and decreases towards the other two corners. In the intermediate layer, at locations sufficiently far away from the inflow (here for $x \gtrsim 0.3$), U varies little with height but primarily with the horizontal coordinate, as illustrated by the near-vertical iso-lines. Moving away from the left wall, U declines so quickly that more than three-fifths of the layer has a velocity magnitude of less than 0.1. Since, according to the scalings (2.5*a–d*), $U = 0.1$ is equal to the plume velocity at the height $y = 1/800$, the induced flow is generally weak compared with the primary plume motion. Though lacking immediate practical interest due to its location, the induced flow pattern in the top layer is distinct and worthy of comment. The bulk flow is the most rapid of the three layers and has a complex distribution of velocity. In the central and right sides of this layer, the velocity magnitude is mainly dependent on the horizontal coordinate (cf. the intermediate layer). Interestingly, along the ceiling, the velocity magnitude has a maximum at $x = 0.15$ (to 2 s.f.), which results directly from the specific profile adopted that accounts for entrainment into the ceiling current, (6.5*a*,*b*).

To gain further insight into how the velocity magnitude varies spatially, figure 8 displays the variation of $U(x = \text{const.}, y)$ along three vertical sections in the box, $x = \{0.25, 0.5, 0.75\}$. For convenience, the depth of each layer is scaled so as to have unit height. The velocity magnitude in the base layer shows more vertical variation, but less horizontal variation than the intermediate and top layers; there is a velocity increase with height on the left side of the box ($x = 0.25$) and a decrease on the right side ($x = 0.75$). For the intermediate layer, all three profiles exhibit low velocity magnitudes (consistent with the large-scale, near-stagnant region reported in § 7.2) and little variation with height. The velocity magnitude in the top layer is generally high (exceeding $U = 0.9$ on $x = 0.25$) while the vertical variation is relatively slight.

7.4. *Controlling the induced flow*

In practical terms, the area of the openings and the room aspect ratio, $\{A/H, \mathcal{A}\}$, are the two key quantities that are available to a ventilation engineer at the design stage to control the induced flow. Since the number of interfaces can be estimated from figure 4, by experience, or by estimating A/H, the two controllable variables are chosen to be n and $\mathcal{A}$ in the following discussion (as is consistent with § 6).

We note from figure 6 that the number of interfaces has little effect on the fundamental pattern of flow in any type of layer but significantly influences the dimensionless velocity magnitude U within the whole box. With more layers, U declines rapidly, which results from the decreasing ventilation flow rate q_0. Take the base layer for instance. The spatially averaged velocity magnitude, $\bar{U}$, defined as the ventilation flow rate divided by layer depth, is

$$\bar{U} := q_0/h_0 \sim h_0^{1/3}. \tag{7.3}$$

The reduction of h_0 with n leads to overall slower motion with correspondingly sparser streamlines. Similar arguments may be applied to the top and intermediate layers.

When n increases from one to three, the velocity magnitude U in the base layer declines almost by half. In the meantime, the stale air region in the intermediate layer widens considerably. Thus, to enhance the natural ventilation, n should be as small as possible, which is primarily achieved with larger effective opening areas A/H.

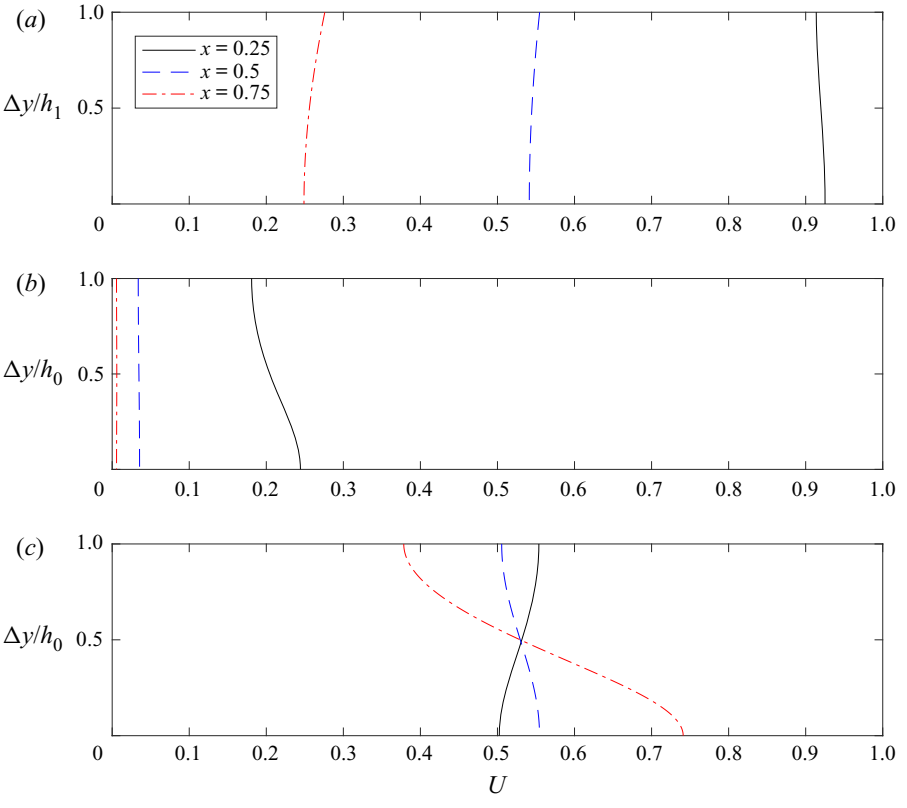

Figure 8. Vertical profiles of dimensionless velocity magnitude U at a quarter ($x = 0.25$), a half ($x = 0.5$) and three quarters ($x = 0.75$) of the box width from the wall plume; $\mathcal{A} = 1$, $n = 2$. (*a*) Top, (*b*) intermediate and (*c*) base layer. Here, Δy denotes the vertical distance from the base of each layer.

Figure 9 highlights the role of box aspect ratio $\mathcal{A}$ in the induced flow for (*a*) $\mathcal{A} = 0.5$ and (*b*) $\mathcal{A} = 1.5$. Evidently, the general flow pattern is weakly dependent on $\mathcal{A}$, which is relatively unchanged despite the factor of three increase in $\mathcal{A}$. There is, however, a marked decrease in the depth of the top layer and increase in the velocity magnitude within the layer. The latter increase is due to the reduced top layer depth transporting the increased volume flux that has resulted from the deepening of the lower layers. By comparison, the velocity magnitude in the lower layers only changes slightly. Interestingly, with increasing $\mathcal{A}$, the streamlines in the base layer indicate an increasingly uniform flow, a desirable characteristic for the ventilation of many rooms. Despite this, there is a widening of the near-stagnant region in the intermediate layer, which is undesirable.

7.5. *A comment on box size and wall buoyancy flux*

The box size, as fully specified by the box height H (m) for a given aspect ratio $\mathcal{A}$, and the source buoyancy flux χ (m^2 s^{-3}) have no effect on the dimensionless induced flow field since they both vanish in the non-dimensionalisation. Nevertheless, on dimensional grounds (2.5*a–d*), the velocity magnitude $U \propto H^{1/3}\chi^{1/3}$ and the buoyancy $g'_e \propto H^{-1/3}\chi^{2/3}$. For given $(n, \mathcal{A})$, there is no change to the pattern of flow on increasing χ or H. However, there will be an increase in the magnitude of the velocity. Moreover, the

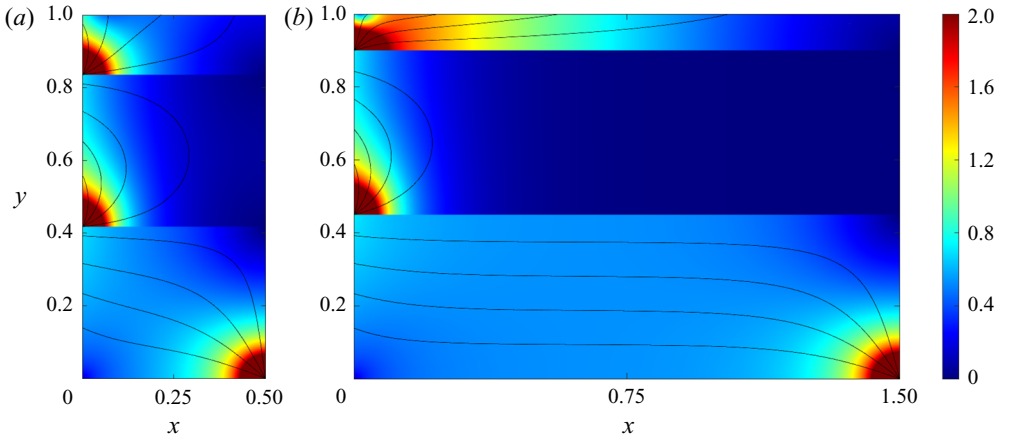

Figure 9. Colour map of dimensionless velocity magnitude $U(x, y)$ overlain with streamline pattern for the $n = 2$ stratification; (*a*) $\mathcal{A} = 0.5$, (*b*) $\mathcal{A} = 1.5$. The step between two adjacent streamlines is $\Delta\psi = 0.05$. The vertical colour bar indicates the magnitude of the dimensionless velocity.

layer buoyancy and the buoyancy jump across each interface increase with χ and decrease with H.

7.6. *Stability of interfaces and instability of ceiling jet*

All solutions above for the induced flow suggest a velocity jump and, thereby, a shear flow at each interface and between the perimeter of the ceiling current and its surroundings. The destabilising influence of the shear competes against the stabilising stratification, potentially leading to a breakdown of the flow through the Kelvin–Helmholtz mechanism. Previously, Cooper & Hunt (2010) suggested that interfacial instability might be the reason that fewer interfaces were observed than predicted. For this reason, it is prudent to assess the stability of the situation we predict via a simplified analysis. The corresponding linear stability criterion, developed by Taylor–Goldstein (Turner 1979, Chapter 4), is well established as

$$\frac{\pi\Delta u^2}{\lambda\Delta g'_e} < 1, \tag{7.4}$$

where Δu and $\Delta g'_e$ denote the jump in the horizontal component of flow velocity and layer buoyancy, and λ is the wavelength of a normal mode perturbation. For stability, the above criterion needs to be satisfied for the longest possible wavelength $\lambda = 2a$, i.e. a wavelength equal to the width of the box.

For each interface $\Delta g'_e = c_1^{-1} h_0^{-1/3}$ from (2.12), and hence (7.4) may be written in terms of an interfacial critical velocity jump, Δu_{crit}

$$\Delta u < \sqrt{\frac{2a}{\pi c_1 h_0^{1/3}}} = \Delta u_{crit}. \tag{7.5}$$

As the velocity jump Δu varies with x (figure 7), the stability situation may vary along each interface. For the ceiling current, stability would require $\Delta u < \Delta u_{crit,ce}$, and we take Δu to be that at the source ($x = 0$, $y = 1$) as here the velocity jump between current, with an average velocity of $q_{ce}(0)/d_{ce}(0)$, and ambient is the greatest.

	Interface(s)		Ceiling current		
n	Δu_{crit}	Stable range (counting from the lowest interface)	$\Delta u_{crit,ce}$	Δu	Unstable
1	0.72	$0.59 < x < 1$	0.81	26	✓
2	0.78	$0.24 < x < 1, 0.25 < x < 1$	0.91	21	✓
3	0.83	$0.14 < x < 1, 0.10 < x < 1, 0.21 < x < 1$	0.99	18	✓

Table 1. Entries (to 2 s.f.) relating to the stability, or otherwise, of the interfaces between layers and the ceiling current. $\mathcal{A} = 1$.

The corresponding stability parameters for $n = 1$, 2 and 3 in a square box are given in table 1. Column three shows that an interface is stable on the right-hand side but linearly unstable on the left-hand side. With the stable locations being marked with solid lines in figure 6, the length of the unstable part increases markedly with decreasing n. While it is likely that viscosity and nonlinear effects stabilise the unstable part of an interface in practice, it should also be noted that criterion (7.4) fails at the left end of an interface because two of the assumptions underlying (7.4), i.e. potential flow and uniform streams, break down there. Comparing columns four and five, $\Delta u \gg \Delta u_{crit,ce}$ is consistent with a turbulent ceiling current.

8. Discussion and conclusion

We considered the steady flow that a turbulent wall plume induces in an emptying–filling box where openings, slots made in the base and top of the box, connect the interior to a uniform, quiescent exterior. Previous developments focus, almost exclusively, on the stratification, modelling this as a stack of equal-depth layers. Our focus has instead been on the development of a simplified theoretical model for predicting the streamline pattern and velocity distribution within the layers. These important aspects of the flow had not been examined previously, either theoretically or experimentally, despite having important practical implications for achieving comfort in naturally ventilated buildings and for the indoor spread of airborne contagions, such as an influenza virus. These flows can be induced in a room by a wall or glass façade heated by the Sun (or for the vertical inversion of the case we consider, cooled by the exterior air) and our primary motivation has been to gain insights into the patterns of flow established in ventilated buildings, together with a grasp of the parameters that control them.

Our contribution is essentially fourfold. First, for the ‘classic’ stratification of equal-depth layers, we developed closed-form solutions for the streamfunction that describe the wall-plume-induced flow within each layer. Second, recognising that the classic stratification neglects the flow near the ceiling, we introduced an entraining ceiling current hypothesis and the corresponding theoretical description of the resulting stratification, removing the need to assume that all layers have equal depth. This re-evaluation of the stratification highlighted the dependence of the layer depths on the entraining current. Third, we solved for the induced flow for the refined stratification and, finally, assessed the implications of our predictions for stratified flows in ventilated rooms. Cooper & Hunt (2010) comment that persistent interfaces are hard to maintain in experiment and, whilst this could be attributed to the challenges of achieving and maintaining a source of uniform and constant buoyancy flux, this provided motivation for us to consider the stability of the interfaces. In principle, the simplified linearised analysis we present serves only to justify that the interfaces can be stable in general cases and, via

this analysis, we can be more confident about the stratification model we present. A full investigation of the interfacial stability, including nonlinear effects and viscosity, would likely offer considerable additional insight although this falls outside the immediate scope of our work.

Working in the complex plane, conformal mapping techniques and Poisson's integral theorem were deployed to solve for the flow induced within each layer, with the boundary conditions established by treating the wall plume as a vertical line of sinks. Advantages of this approach over alternatives include the ability to rapidly re-evaluate the solution on altering the dimensions and locations of the openings (appendix A), and the ease with which multiple additional openings can be included.

In existing emptying–filling-box studies, where turbulent entrainment occurs solely over the vertical rise of the plume, layer depths depend exclusively on the dimensionless effective opening area. The inclusion of an entraining horizontal current reveals an additional dependence, namely, on the box aspect ratio $\mathcal{A} = W/H$, taken herein as width relative to height, and a top layer that is thinner than the other layers and which adjusts in depth with effective opening area. According to our model, the layers can only have equal depth if there is no entrainment by the ceiling current. Increasing $\mathcal{A}$ causes a reduction in the depth of the top layer and an increase in the depth of the layers below, while the number of interfaces n shows a weak tendency to increase with $\mathcal{A}$. Overlooking the ceiling current, which contributes significantly to overall entrainment, the classic model of stratification leads to an underestimation of the ventilation flow rate.

The flow patterns characterising the base layer, intermediate layer(s) and top layer that comprise the stratification each have distinguishing characteristics which vary only quantitatively with n and $\mathcal{A}$. The source buoyancy flux χ (m^2 s^{-3}) and box size (referring to box height H (m) for a given aspect ratio) have no influence on the patterns of flow but determine the velocity magnitude, which scales as $\chi^{1/3}$ and $H^{1/3}$. Consistent with the classic stratification, the dimensionless velocity magnitude declines significantly in each layer with n. Moreover, the buoyancy of the top and intermediate layers increases with χ but decreases with H.

Although our wall-jet hypothesis excludes the effect of the stratification on the ceiling current, and thus may overestimate entrainment, this has little impact on the prediction of the induced flow pattern within the lower layers which is of paramount interest for the application to room ventilation. While there is evidence that a lateral ceiling current produces mixing along its perimeter (e.g. Kaye & Hunt 2007), there are currently no detailed measurements that we are aware of that are specific to the wall-plume emptying–filling box considered herein. Beyond the unresolved complication of achieving a uniform source buoyancy flux and that specifying the effective opening area *a priori* is simply not possible, analogue experiments (cf. Cooper & Hunt 2010) are notoriously difficult to conduct and so a more detailed quantitative validation of our predictions is not currently possible. Even so, we have smoothly varying predictions of stratification across a spectrum of effective opening areas and gained a first insight into the streamline pattern and velocity distribution. That stated, our approach is simplified, and although, according to Cooper & Hunt (2010), experimental difficulties lead to a departure from the target, idealised wall-plume boundary conditions, some of the previous experiments exhibited vertical density gradients within layers and evidence of detrainment from the wall plume (Gladstone & Woods 2014). As such, we suggest that the current model be applied in cases when entrainment is dominant along the wall plume, i.e. for a wall plume with relatively high local Richardson numbers.

Finally, from the perspective of airflow in buildings, both in terms of achieving comfort for natural ventilation and with regards to the movement of passive airborne contaminants

or fine aerosol mists by the induced flow, our results indicate that (i) the choice of location of the lower opening is crucial to successfully ventilating the lower layer given it can lead to a desirable smooth flushing of this region or to a large-scale region of near-stagnant air and (ii) intermediate layers are characterised by large-scale stagnant regions, irrespective of opening location. We end with a cautionary note regarding the direct application of our work to room ventilation where the movement of occupants, an external wind flow or variations in the solar heat gains received by a façade would cause a departure from the idealised, albeit already complex, steady situation we have considered. Whilst this idealisation has offered new insights into the airflow patterns induced and a simplified predictive capability, the situation in practice is unquestionably far more complex and such well-defined layers may not form.

Acknowledgements. The authors are grateful to three anonymous referees for their helpful comments on an earlier draft.

Funding. G.R.H. would like to express his gratitude to Dyson Technology Ltd for their ongoing support and to the EPSRC through grant no. EP/N010221/1, entitled Managing Air for Green Inner Cities (MAGIC).

Declaration of interests. The authors report no conflict of interest.

Author ORCIDs.
Ziheng Yu https://orcid.org/0000-0002-3449-9896;
Gary R. Hunt https://orcid.org/0000-0001-9875-9274.

Appendix A. Wider applicability: general configurations and finite-width openings

By contrast with alternative methods of solution, e.g. separation of variables, the conformal mapping approach developed above can be applied with ease to obtain closed-form solutions for the streamline pattern in emptying–filling boxes with openings of arbitrary width and location. The general form of the induced flow solution (4.7), as expressed in terms of $\Psi(\xi, 0)$, for each layer in the mapped domain is unchanged. It is convenient here to express this solution as

$$\Psi(u, v) = \frac{v}{\pi}(I_1 + I_2 + I_3 + I_4 + I_5), \tag{A1}$$

where $I_k\,(k = 1, \ldots, 5)$ refers, in order, to the five integrals in (4.7). In the classic configuration, $\Psi(\xi, 0)$ is determined from the boundary conditions (4.4) for the base layer, (4.5) for an intermediate layer and (7.2) for the top layer.

For a lower opening centred on $x = x_l$ with finite width a_l, with the stratification unaffected, only the boundary condition along the base of the box needs to be modified. With the classic high Reynolds number assumption of a uniform inflow velocity profile, the original boundary condition at the lower opening is replaced with a linearly varying streamfunction. Thus, only the solution for the base layer is altered and this change is

$$I_3 = \int_{\xi_1}^{\xi_2} -\frac{q_0}{a_l}\left(C\,\mathrm{sn}^{-1}\xi - x_l + \frac{a_l + 1}{2}\right)\mathrm{d}\xi + \int_{\xi_2}^{1} -q_0\,\mathrm{d}\xi, \tag{A2}$$

where $\xi_1 = \mathrm{sn}((x_l - a_l/2)/C)$ and $\xi_2 = \mathrm{sn}((x_l + a_l/2)/C)$. To acquire the solutions plotted in figure 10(*a–c*), one needs to substitute into (A2): (*a*) $x_l = 0.5$ and $a_l = 0$; (*b*) $x_l = 0.925$ and $a_l = 0.15$; and (*c*) $x_l = 0.5$ and $a_l = 0.15$, respectively.

For an upper opening centred at $x = x_u$, the formulation of a practical boundary condition at the ceiling, accounting for the interaction of the current with buoyancy-driven flow toward the opening, would appear to be extremely complicated and beyond the scope

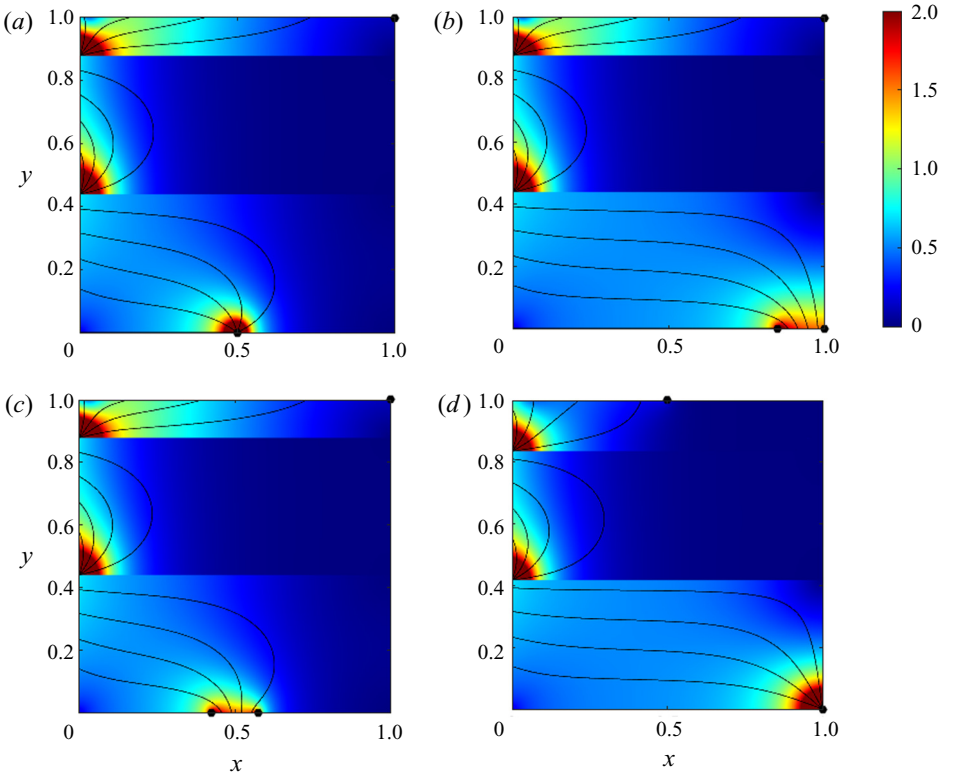

Figure 10. Streamlines superimposed on a colour map of velocity magnitude for four opening configurations in a square box with $n = 2$. The buoyancy source is uniformly distributed along the left wall (y-axis). The deviations from the opening configurations examined in §§ 6 and 7 are (*a*) lower opening moved to mid-point of base, (*b*) lower opening of finite width 0.15, (*c*) lower opening of finite width 0.15 centred at mid-point of base and (*d*) top opening moved to mid-point of ceiling. The black dots indicate opening location and width. The increment between adjacent streamlines is $\Delta\psi = 0.05$.

of this study. Indeed, not only could the current horizontally overshoot the location of the upper opening but the variation of volume flux across the opening, affected by the outflow, is expected to deviate considerably from that of the ceiling jet. However, to demonstrate the applicability of our solution approach, we adopt the boundary condition for an 'ideal' ceiling current which drains out totally through a point opening without horizontal overshooting. The stratification needs to be re-determined by replacing (6.1) with $q_{ce}(x_u) = q_0$, thereby accounting for the reduction in entrainment along the ceiling current. Based on the updated stratification, the boundary condition at locations to the right of the upper opening becomes $\psi = -q_0$. Only the induced flow solution for the top layer is altered. Defining $\xi_3 = \mathrm{sn}((x_u - 1/2 + \mathrm{i}h_1)/C)$, the change, with reference to (A1), is

$$I_1 = \int_{-\infty}^{\xi_3} -q_0 \,\mathrm{d}\xi + \int_{\xi_3}^{-1} -c_2 q_0 \sqrt{\frac{2(C\,\mathrm{sn}^{-1}(u) + a + 1/2 - \mathrm{i}h_1)}{3\alpha h_1} + \frac{1}{c_2^2}}\,\mathrm{d}\xi, \tag{A3}$$

when $x_u \leqslant 0.5$, or

$$I_5 = \int_{1}^{\xi_3} -q_0 \,\mathrm{d}\xi + \int_{\xi_3}^{\infty} -c_2 q_0 \sqrt{\frac{2(C\,\mathrm{sn}^{-1}(u) + a + 1/2 - \mathrm{i}h_1)}{3\alpha h_1} + \frac{1}{c_2^2}}\,\mathrm{d}\xi, \tag{A4}$$

when $x_u > 0.5$. Substituting $x_u = 0.5$ into (A3) leads to the solution shown in figure 10(*d*).

A few features of the induced flows generated with these opening configurations in figure 10 are worthy of mention. First is the appearance of a region of near-stagnant fluid forming to the right side of the opening in the base layer on moving the lower opening (figure 10*a*,*c*). Second, if not too wide ($a_l \ll 1$), the width of a lower opening does not significantly alter the induced flow pattern (compare figure 10*a* with 10*c*), other than adjacent to the opening.

References

Abedin, M.Z., Tsuji, T. & Hattori, Y. 2009 Direct numerical simulation for a time-developing natural-convection boundary layer along a vertical flat plate. *Intl J. Heat Mass Transfer* **52** (19–20), 4525–4534.

Baines, W.D. & Turner, J.S. 1969 Turbulent buoyant convection from a source in a confined region. *J. Fluid Mech.* **37** (1), 51–80.

Bonnebaigt, R., Caulfield, C.P. & Linden, P.F. 2018 Detrainment of plumes from vertically distributed sources. *Environ. Fluid Mech.* **18** (1), 3–25.

Caudwell, T., Flór, J.-B. & Negretti, M.-E. 2016 Convection at an isothermal wall in an enclosure and establishment of stratification. *J. Fluid Mech.* **799**, 448–475.

Cooper, P. & Hunt, G.R. 2010 The ventilated filling box containing a vertically distributed source of buoyancy. *J. Fluid Mech.* **646**, 39–58.

Cooper, P. & Linden, P.F. 1996 Natural ventilation of an enclosure containing two buoyancy sources. *J. Fluid Mech.* **311**, 153–176.

Driscoll, T.A. & Trefethen, L.N. 2002 *Schwarz-Christoffel Mapping*. Cambridge University Press.

George, S.P. Jr. & Capp, W.K. 1979 A theory for natural convection turbulent boundary layers next to heated vertical surfaces. *Intl J. Heat Mass Transfer* **22** (6), 813–826.

Gladstone, C. & Woods, A.W. 2001 On buoyancy-driven natural ventilation of a room with a heated floor. *J. Fluid Mech.* **441**, 293–314.

Gladstone, C. & Woods, A.W. 2014 Detrainment from a turbulent plume produced by a vertical line source of buoyancy in a confined, ventilated space. *J. Fluid Mech.* **742**, 35–49.

Heiselberg, P. & Sandberg, M. 1990 Convection from a slender cylinder in a ventilated room. In *Proceedings of Roomvent '90, Oslo, Norway, June 13–15* (ed. K. Svidt).

Holford, J.M. & Hunt, G.R. 2001 The dependence of the discharge coefficient on density contrast–experimental measurements. In *Proceedings 14th Australasian Fluid Mechanics Conference* (ed. B.B. Dally), pp. 123–126.

Hunt, G.R. & Coffey, C.J. 2010 Emptying boxes-classifying transient natural ventilation flows. *J. Fluid Mech.* **646**, 137–168.

Hunt, G.R. & Holford, J.M. 2000 The discharge coefficient–experimental measurement of a dependence on density contrast. In *Proceedings of the 21st AIVC Conference, The Hague, Netherlands*.

Hunt, G.R. & Linden, P.F. 2001 Steady-state flows in an enclosure ventilated by buoyancy forces assisted by wind. *J. Fluid Mech.* **426**, 355–386.

Hunt, G.R. & Linden, P.F. 2005 Displacement and mixing ventilation driven by opposing wind and buoyancy. *J. Fluid Mech.* **527**, 27–55.

Kaye, N.B. & Cooper, P. 2018 Source and boundary condition effects on unconfined and confined vertically distributed turbulent plumes. *J. Fluid Mech.* **850**, 1032–1065.

Kaye, N.B. & Hunt, G.R. 2007 Overturning in a filling box. *J. Fluid Mech.* **576**, 297–323.

Kerr, R.C. & McConnochie, C.D. 2015 Dissolution of a vertical solid surface by turbulent compositional convection. *J. Fluid Mech.* **765**, 211–228.

Kotsovinos, N.E. 1977 Plane turbulent buoyant jets. Part 2. Turbulence structure. *J. Fluid Mech.* **81** (1), 45–62.

Linden, P.F. 1999 The fluid mechanics of natural ventilation. *Annu. Rev. Fluid Mech.* **31** (1), 201–238.

Linden, P.F. & Cooper, P. 1996 Multiple sources of buoyancy in a naturally ventilated enclosure. *J. Fluid Mech.* **311**, 177–192.

Linden, P.F., Lane-Serff, G.F. & Smeed, D.A. 1990 Emptying filling boxes: the fluid mechanics of natural ventilation. *J. Fluid Mech.* **212**, 309–335.

Loganathan, R.M. & Hunt, G.R. 2019 Analytical solutions for flow induced by a vertically distributed turbulent plume. *Environ. Fluid Mech.* **19** (4), 801–818.

McBain, G.D., Armfield, S.W. & Desrayaud, G. 2007 Instability of the buoyancy layer on an evenly heated vertical wall. *J. Fluid Mech.* **587**, 453–469.

MORTON, B.R., TAYLOR, G. & TURNER, J.S. 1956 Turbulent gravitational convection from maintained and instantaneous sources. *Proc. R. Soc. Lond.* A **234** (1196), 1–23.
RAJARATNAM, N. 1976 *Turbulent Jets*. Elsevier.
TAYLOR, G. 1958 Flow induced by jets. *J. Aerosp. Sci.* **25** (7), 464–465.
TSUJI, T. & NAGANO, Y. 1989 Velocity and temperature measurements in a natural convection boundary layer along a vertical flat plate. *Exp. Therm. Fluid Sci.* **2** (2), 208–215.
TURNER, J.S. 1979 *Buoyancy Effects in Fluids*. Cambridge University Press.
WARD-SMITH, A.J. 1980 *Internal Fluid Flow: the Fluid Dynamics of Flow in Pipes and Ducts*. Clarendon Press.
WISE, N.H. & HUNT, G.R. 2020 Buoyancy-driven unbalanced exchange flow through a horizontal opening. *J. Fluid Mech.* **888**, A22.
YIH, C.-S. 1980 *Stratified Flows*. Academic.